J|A|C|S
ARTICLES

Published on Web 12/23/2008

Engineering of Supramolecular H-Bonded Nanopolygons via Self-Assembly of Programmed Molecular Modules

Anna Llanes-Pallas,[†] Carlos-Andres Palma,[‡] Luc Piot,[‡] Abdelhalim Belbakra,[§] Andrea Listorti,[§] Maurizio Prato,[†] Paolo Samorì,*[,§,‡] Nicola Armaroli,*[,§] and Davide Bonifazi*[,†,||]

Università degli Studi di Trieste, Dipartimento di Scienze Farmaceutiche and INSTM UdR di Trieste, Piazzale Europa 1, 34127 Trieste, Italy, ISIS-CNRS 7006, Université Louis Pasteur, 8 allée Gaspard Monge, 67000 Strasbourg, France, Istituto per la Sintesi Organica e la Fotoreattività (ISOF), Consiglio Nazionale delle Ricerche, Via Gobetti 101, 40129 Bologna, Italy, and University of Namur (FUNDP), Department of Chemistry, Rue de Bruxelles 61, 5000 Namur, Belgium

Received June 20, 2008; E-mail: samori@isis-ulp.org; nicola.armaroli@isof.cnr.it; davide.bonifazi@fundp.ac.be

Abstract: Discrete and multicomponent nanoscale noncovalent assemblies on surfaces featuring polygonal porous domains are presented. The molecular engineering concept involves multivalent molecular modules that are preprogrammed to undergo heteromolecular recognition by exploiting complementary multiple H bonds. Two types of molecular modules have been engineered: (*i*) a linear unit of twofold symmetry exposing two 2,6-di(acylamino)pyridyl [donor−acceptor−donor (DAD)] recognition sites at its extremities with a 180° orientation relative to each other and (*ii*) an angular unit constituted by a 1,3,6,8-tetraethynylpyrene core peripherally functionalized with four uracil groups [acceptor−donor−acceptor (ADA)] positioned at 60° and 120° relative to each other. These molecular modules self-assemble through H-bonds between the complementary recognition sites, forming supramolecular architectures. Their symmetry depends upon the type of each individual subunit and the stoichiometry as well as on the combination and distribution of the main symmetry axes. These so-formed two-dimensional (2D) supramolecular oligomers have been studied in solution by optical spectroscopy and on highly ordered pyrolitic graphite (HOPG) substrates by scanning tunneling microscopy (STM) at the solid−liquid interface. Steady-state UV/vis absorption and emission titration measurements suggest the reversible formation of multiple oligomeric species with slightly modulated fluorescence spectra. This likely reflects the presence of various aggregates between the two polytopic receptors, which exhibit somewhat different electronic delocalization as a function of the aggregate size. The presence of multiple species is further confirmed by time-resolved luminescence measurements: lifetime values are fitted as double/multiple exponentials and are always shorter than 6.5 ns. The formation of several oligomeric species is further supported by in situ STM measurements at the solid−liquid interface that provided evidence, with submolecular resolution, for the formation of multicomponent and discrete 2D polygon-like assemblies. We highlight the role of accurate control of the concentration required to image on the surface the 2D oligomeric species formed in solution, which allows us to bypass the determinant role of the substrate−molecule interactions in forming the thermodynamically stable monocomponent architectures at the solid−liquid interface.

Introduction

Organic-based materials originate from the need to engineer matter at the molecular level,[1−6] resulting in advanced materials that hold great promise for successful applications in many fields, such as electronics,[7−12] optoelectronics,[13−16] photonics,[17] and energy storage.[18,19] The ability to control matter at the molecular level with specific molecular functional systems constitutes one of the challenges in the field of nanoscience.[20−22]

[†] UNITS.
[‡] ISIS-CNRS.
[§] ISOF-CNR.
[||] FUNDP.

(1) Grimsdale, A. C.; Müllen, K. *Angew. Chem., Int. Ed.* **2005**, *44*, 5592.
(2) Hoeben, F. J. M.; Jonkheijm, P.; Meijer, E. W.; Schenning, A. *Chem. Rev.* **2005**, *105*, 1491.
(3) Palermo, V.; Samorì, P. *Angew. Chem., Int. Ed.* **2007**, *46*, 4428.
(4) Vriezema, D. M.; Aragones, M. C.; Elemans, J. A. A. W.; Cornelissen, J. J. L. M.; Rowan, A. E.; Nolte, R. J. M. *Chem. Rev.* **2005**, *105*, 1445.
(5) Stupp, S. I.; LeBonheur, V.; Walker, K.; Li, L. S.; Huggins, K. E.; Keser, M.; Amstutz, A. *Science* **1997**, *276*, 384.
(6) van Hameren, R.; Schon, P.; van Buul, A. M.; Hoogboom, J.; Lazarenko, S. V.; Gerritsen, J. W.; Engelkamp, H.; Christianen, P. C. M.; Heus, H. A.; Maan, J. C.; Rasing, T.; Speller, S.; Rowan, A. E.; Elemans, J. A. A. W.; Nolte, R. J. M. *Science* **2006**, *314*, 1433.
(7) Schenning, A.; Meijer, E. W. *Chem. Commun.* **2005**, 3245.
(8) Green, J. E.; Choi, J. W.; Boukai, A.; Bunimovich, Y.; Johnston-Halperin, E.; DeIonno, E.; Luo, Y.; Sheriff, B. A.; Xu, K.; Shin, Y. S.; Tseng, H. R.; Stoddart, J. F.; Heath, J. R. *Nature* **2007**, *445*, 414.
(9) Wu, J. S.; Pisula, W.; Müllen, K. *Chem. Rev.* **2007**, *107*, 718.
(10) Murphy, A. R.; Fréchet, J. M. J. *Chem. Rev.* **2007**, *107*, 1066.
(11) Haick, H.; Cahen, D. *Acc. Chem. Res.* **2008**, *41*, 359.
(12) Yang, H. C.; Shin, T. J.; Yang, L.; Cho, K.; Ryu, C. Y.; Bao, Z. N. *Adv. Funct. Mater.* **2005**, *15*, 671.

To develop such materials, the hierarchical self-assembly of multivalent components through the concerted action of multiple noncovalent interactions turns out to be one of the most promising approaches, as it allows the simultaneous organization of discrete molecules, long-range order, and inherently defect-free structures.[23−27] The structural and functional properties of the final supramolecular architectures result from the information stored in their molecular components, which is dictated by the interplay of conformational and geometrical constraints and by the presence of specific functional moieties.[28] One of the major problems in working with nanostructured materials is that the matter can no longer be considered as a bulk entity, since the molecular components need to be addressed at the single-molecule level.[29] As a consequence, widely employed engineering methodologies in nanotechnology use inert surfaces as supporting substrates in the assembly of supramolecular networks. In this regard, the now mature scanning probe microscopy (SPM) techniques, especially scanning tunneling microscopy (STM) at the solid−liquid interface, enable the nanoscale characterization of these molecule-based 2D supramolecular architectures in direct space.[30−46]

A classical approach to the formation of 2D supramolecular networks via spontaneous self-assembly of molecular modules is to use weak yet highly directional interactions, such as H-bonds, that provide a powerful handle for the engineering and design of supramolecular assemblies by reducing the effect of nonspecific intermolecular interactions (e.g., of the van der Waals type). Although this methodology has been widely and successfully employed in the preparation of monocomponent networks,[47−60] it has been less explored in the self-assembly of large programmed bicomponent[61−71] architectures. In order to achieve complete control over the 2D structure and properties in dynamic media (i.e., at the solid−liquid interface), it is also important to understand the interplay between the molecule−

(13) Friend, R. H.; Gymer, R. W.; Holmes, A. B.; Burroughes, J. H.; Marks, R. N.; Taliani, C.; Bradley, D. D. C.; Dos Santos, D. A.; Brédas, J. L.; Logdlund, M.; Salaneck, W. R. *Nature* **1999**, *397*, 121.
(14) Forrest, S. R. *Nature* **2004**, *428*, 911.
(15) Cacialli, F.; Wilson, J. S.; Michels, J. J.; Daniel, C.; Silva, C.; Friend, R. H.; Severin, N.; Samorì, P.; Rabe, J. P.; O'Connell, M. J.; Taylor, P. N.; Anderson, H. L. *Nat. Mater.* **2002**, *1*, 160.
(16) Yamamoto, Y.; Fukushima, T.; Suna, Y.; Ishii, N.; Saeki, A.; Seki, S.; Tagawa, S.; Taniguchi, M.; Kawai, T.; Aida, T. *Science* **2006**, *314*, 1761.
(17) Ajayaghosh, A.; Praveen, V. K. *Acc. Chem. Res.* **2007**, *40*, 644.
(18) Gunes, S.; Neugebauer, H.; Sariciftci, N. S. *Chem. Rev.* **2007**, *107*, 1324.
(19) Arico, A. S.; Bruce, P.; Scrosati, B.; Tarascon, J. M.; Van Schalkwijk, W. *Nat. Mater.* **2005**, *4*, 366.
(20) Philp, D.; Stoddart, J. F. *Angew. Chem., Int. Ed. Engl.* **1996**, *35*, 1154.
(21) Whitesides, G. M.; Mathias, J. P.; Seto, C. T. *Science* **1991**, *254*, 1312.
(22) *Science* **2002**, *295*, 2396 (special issue on "Supramolecular Chemistry and Self-Assembly").
(23) Bonifazi, D.; Kiebele, A.; Stöhr, M.; Cheng, F.; Jung, T.; Diederich, F.; Spillmann, H. *Adv. Funct. Mater.* **2007**, *17*, 1051.
(24) Barth, J. V. *Annu. Rev. Phys. Chem.* **2007**, *58*, 375.
(25) Barth, J. V.; Costantini, G.; Kern, K. *Nature* **2005**, *437*, 671.
(26) Rosei, F.; Schunack, M.; Naitoh, Y.; Jiang, P.; Gourdon, A.; Laegsgaard, E.; Stensgaard, I.; Joachim, C.; Besenbacher, F. *Prog. Surf. Sci.* **2003**, *71*, 95.
(27) Rosei, F. *J. Phys.: Condens. Matter* **2004**, *16*, S1373.
(28) *Chem. Rev.* **2005**, *105*, 1023−1562 (special issue on "Functional Nanostructures").
(29) Gimzewski, J. K.; Joachim, C. *Science* **1999**, *283*, 1683.
(30) De Feyter, S.; De Schryver, F. C. *J. Phys. Chem. B* **2005**, *109*, 4290.
(31) Piot, L.; Bonifazi, D.; Samorì, P. *Adv. Funct. Mater.* **2007**, *17*, 3689.
(32) Surin, M.; Samorì, P. *Small* **2007**, *3*, 190.
(33) Otero, R.; Rosei, F.; Besenbacher, F. *Annu. Rev. Phys. Chem.* **2006**, *57*, 497.
(34) Hermann, B. A.; Scherer, L. J.; Housecroft, C. E.; Constable, E. C. *Adv. Funct. Mater.* **2006**, *16*, 221.
(35) Cyr, D. M.; Venkataraman, B.; Flynn, G. W. *Chem. Mater.* **1996**, *8*, 1600.
(36) Giancarlo, L. C.; Flynn, G. W. *Acc. Chem. Res.* **2000**, *33*, 491.
(37) Rabe, J. P.; Buchholz, S. *Science* **1991**, *253*, 424.
(38) Mena-Osteritz, E. *Adv. Mater.* **2002**, *14*, 609.
(39) Furukawa, S.; Uji-i, H.; Tahara, K.; Ichikawa, T.; Sonoda, M.; De Schryver, F. C.; Tobe, Y.; De Feyter, S. *J. Am. Chem. Soc.* **2006**, *128*, 3502.
(40) Lei, S. B.; Tahara, K.; De Schryver, F. C.; Van der Auweraer, M.; Tobe, Y.; De Feyter, S. *Angew. Chem., Int. Ed.* **2008**, *47*, 2964.
(41) Schull, G.; Douillard, L.; Fiorini-Debuisschert, C.; Charra, F.; Mathevet, F.; Kreher, D.; Attias, A. J. *Nano Lett.* **2006**, *6*, 1360.
(42) Wan, L. J. *Acc. Chem. Res.* **2006**, *39*, 334.
(43) Wei, Y. H.; Kannappan, K.; Flynn, G. W.; Zimmt, M. B. *J. Am. Chem. Soc.* **2004**, *126*, 5318.
(44) Hulsken, B.; Van Hameren, R.; Gerritsen, J. W.; Khoury, T.; Thordarson, P.; Crossley, M. J.; Rowan, A. E.; Nolte, R. J. M.; Elemans, J. A. A. W.; Speller, S. *Nat. Nanotechnol.* **2007**, *2*, 285.
(45) Bonifazi, D.; Spillmann, H.; Kiebele, A.; de Wild, M.; Seiler, P.; Cheng, F. Y.; Guntherodt, H. J.; Jung, T.; Diederich, F. *Angew. Chem., Int. Ed.* **2004**, *43*, 4759.
(46) Cicoira, F.; Santato, C.; Rosei, F. *Top. Curr. Chem.* **2008**, *285*, 203.
(47) Barth, J. V.; Weckesser, J.; Cai, C. Z.; Gunter, P.; Burgi, L.; Jeandupeux, O.; Kern, K. *Angew. Chem., Int. Ed.* **2000**, *39*, 1230.
(48) De Feyter, S.; Gesquiere, A.; Abdel-Mottaleb, M. M.; Grim, P. C. M.; De Schryver, F. C.; Meiners, C.; Sieffert, M.; Valiyaveettil, S.; Müllen, K. *Acc. Chem. Res.* **2000**, *33*, 520.
(49) Griessl, S.; Lackinger, M.; Edelwirth, M.; Hietschold, M.; Heckl, W. M. *Single Mol.* **2002**, *3*, 25.
(50) Lu, J.; Zeng, Q. D.; Wang, C.; Zheng, Q. Y.; Wan, L. J.; Bai, C. L. *J. Mater. Chem.* **2002**, *12*, 2856.
(51) Giorgi, T.; Lena, S.; Mariani, P.; Cremonini, M. A.; Masiero, S.; Pieraccini, S.; Rabe, J. P.; Samorì, P.; Spada, G. P.; Gottarelli, G. *J. Am. Chem. Soc.* **2003**, *125*, 14741.
(52) Yoshimoto, S.; Yokoo, N.; Fukuda, T.; Kobayashi, N.; Itaya, K. *Chem. Commun.* **2006**, 500.
(53) Pawin, G.; Wong, K. L.; Kwon, K. Y.; Bartels, L. *Science* **2006**, *313*, 961.
(54) Zhou, H.; Dang, H.; Yi, J. H.; Nanci, A.; Rochefort, A.; Wuest, J. D. *J. Am. Chem. Soc.* **2007**, *129*, 13774.
(55) Ma, Z.; Wang, Y. Y.; Wang, P.; Huang, W.; Li, Y. B.; Lei, S. B. *ACS Nano* **2007**, *1*, 160.
(56) Stöhr, M.; Wahl, M.; Galka, C. H.; Riehm, T.; Jung, T. A.; Gade, L. H. *Angew. Chem., Int. Ed.* **2005**, *44*, 7394.
(57) Gottarelli, G.; Masiero, S.; Mezzina, E.; Pieraccini, S.; Rabe, J. P.; Samorì, P.; Spada, G. P. *Chem.—Eur. J.* **2000**, *6*, 3242.
(58) Tao, F.; Bernasek, S. L. *Langmuir* **2007**, *23*, 3513.
(59) Xu, L. P.; Gong, J. R.; Wan, L. J.; Jiu, T. G.; Li, Y. L.; Zhu, D. B.; Deng, K. *J. Phys. Chem. B* **2006**, *110*, 17043.
(60) Meier, C.; Ziener, U.; Landfester, K.; Weihrich, P. *J. Phys. Chem. B* **2005**, *109*, 21015.
(61) De Feyter, S.; Miura, A.; Yao, S.; Chen, Z.; Würthner, F.; Jonkheijm, P.; Schenning, A.; Meijer, E. W.; De Schryver, F. C. *Nano Lett.* **2005**, *5*, 77.
(62) Theobald, J. A.; Oxtoby, N. S.; Phillips, M. A.; Champness, N. R.; Beton, P. H. *Nature* **2003**, *424*, 1029.
(63) Perdigao, L. M. A.; Perkins, E. W.; Ma, J.; Staniec, P. A.; Rogers, B. L.; Champness, N. R.; Beton, P. H. *J. Phys. Chem. B* **2006**, *110*, 12539.
(64) Mourran, A.; Ziener, U.; Möller, M.; Suarez, M.; Lehn, J. M. *Langmuir* **2006**, *22*, 7579.
(65) Xu, W.; Dong, M. D.; Gersen, H.; Rauls, E.; Vazquez-Campos, S.; Crego-Calama, M.; Reinhoudt, D. N.; Stensgaard, I.; Laegsgaard, E.; Linderoth, T. R.; Besenbacher, F. *Small* **2007**, *3*, 854.
(66) Ruiz-Oses, M.; Gonzalez-Lakunza, N.; Silanes, I.; Gourdon, A.; Arnau, A.; Ortega, J. E. *J. Phys. Chem. B* **2006**, *110*, 25573.
(67) Cañas-Ventura, M. E.; Xiao, W.; Wasserfallen, D.; Müllen, K.; Brune, H.; Barth, J. V.; Fasel, R. *Angew. Chem., Int. Ed.* **2007**, *46*, 1814.
(68) Nath, K. G.; Ivasenko, O.; Miwa, J. A.; Dang, H.; Wuest, J. D.; Nanci, A.; Perepichka, D. F.; Rosei, F. *J. Am. Chem. Soc.* **2006**, *128*, 4212.
(69) Eichhorst-Gerner, K.; Stabel, A.; Moessner, G.; Declerq, D.; Valiyaveettil, S.; Enkelmann, V.; Müllen, K.; Rabe, J. P. *Angew. Chem., Int. Ed. Engl.* **1996**, *35*, 1492.
(70) Madueno, R.; Raisanen, M. T.; Silien, C.; Buck, M. *Nature* **2008**, *454*, 618.
(71) Llanes-Pallas, A.; Matena, M.; Jung, T.; Prato, M.; Stöhr, M.; Bonifazi, D. *Angew. Chem., Int. Ed.* **2008**, *47*, 7726.

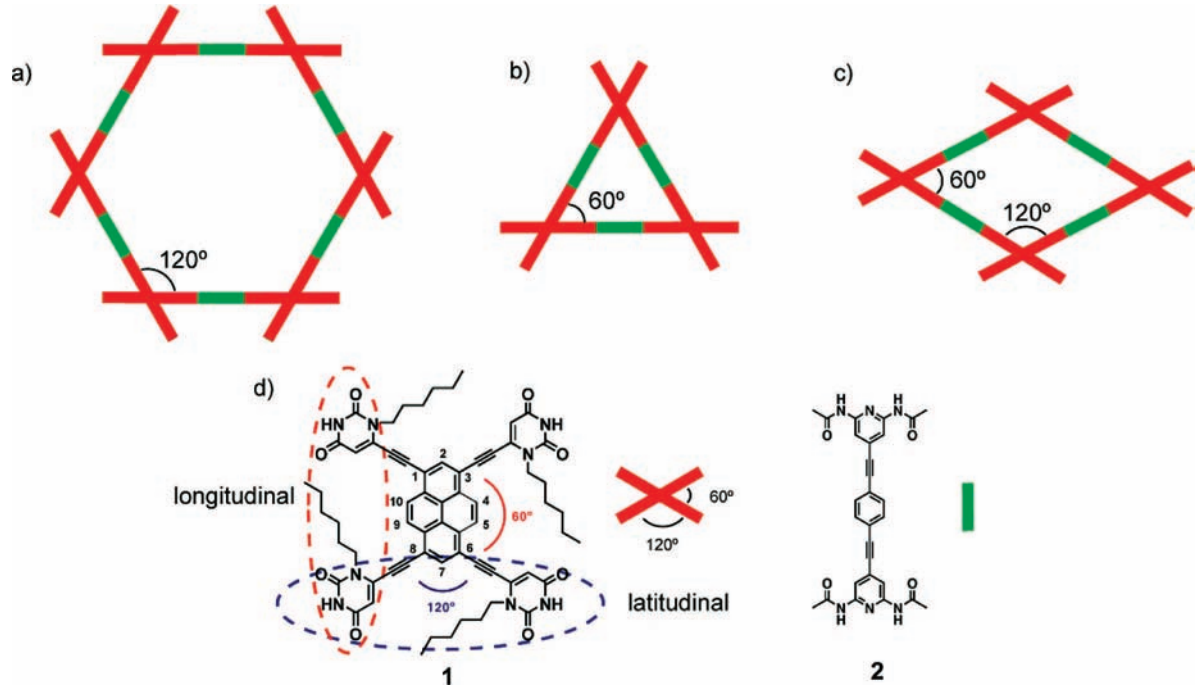

Figure 1. (a−c) Possible polygonal networks obtained by combining the tetratopic and ditopic modules **1** (red) and **2** (green), respectively. (d) Chemical structures and representative cartoons of the modules.

solvent and molecule−substrate interactions governing the process of self-assembly at surfaces.[72−75]

Here we describe the engineering of discrete, molecular-scale, H-bonded assemblies nucleated in solution that have been studied at the solid−liquid interface using a concentration-based approach that allows the visualization of bicomponent 2D hollow structures of different geometries. Two important factors have been considered in the rational design of such supramolecular architectures: (*i*) the symmetry and (*ii*) the binding capabilities (and thus the functionality) of the building blocks. The overall shape of the resulting supramolecular assembly is then a consequence of these parameters.[76] To accomplish this goal, two types of conformationally rigid geometrical modules (angular and linear) equipped with multiple complementary H-bonding sites have been synthesized (Figure 1). Specifically, a 1,3,6,8-tetraethynylpyrene **1** with four exposed uracil groups [acceptor−donor−acceptor (ADA)] positioned at 60° and 120° relative to each other[77] has been designed to interact with a complementary linear module, a 1,4-diethynyl benzene derivative **2** bearing two 2,6-di(acylamino)pyridyl units [donor−acceptor−donor (DAD)], through triple H bonds. Steady-state UV/vis absorption and emission titration measurements suggest the reversible formation of multiple oligomeric species with slightly modulated fluorescence spectra, reflecting the presence of various assemblies between the two polytopic receptors. The presence of multiple species is further confirmed by luminescence lifetime decays that are fitted as double/multiple exponentials. The generation of several oligomeric assemblies featuring hollow structures has been observed at surfaces using in-situ STM measurements at the solid−liquid interface. Despite the fact that the thermodynamics of formation of supramolecular oligomers in solution and on the surface are significantly different in nature, it is usually very difficult to direct the deposition of two or more molecules on a surface, consequently driving the formation of discrete geometrical assemblies because of the difference in adsorption energies[78,79] of the components and their tendency to minimize the occupied area. To this end, low-concentration solutions have been used as a strategy to prevent competitive adsorption,[80−82] thus operating in a regime where the packing is ruled only by the intermolecular interactions, thereby neglecting the role of substrate−molecule interactions. This allowed the simultaneous physisorption of molecules **1** and **2** at the interface, which revealed the formation of discrete polygon-like nanoassemblies featuring hollow structures with a submolecular resolution, therefore providing a direct insight into the complex self-recognition behavior on highly oriented pyrolitic graphite (HOPG).

Results and Discussion

Synthesis. The synthesis of modules **1** and **2** is outlined in Scheme 1. Both modules were synthesized via palladium-catalyzed Sonogashira cross-coupling reactions[83] between the complementary H-bonding recognition units and the corre-

(72) Samorì, P.; Severin, N.; Müllen, K.; Rabe, J. P. *Adv. Mater.* **2000**, *12*, 579.
(73) Gesquiere, A.; Abdel-Mottaleb, M. M.; De Feyter, S.; De Schryver, F. C.; Sieffert, M.; Müllen, K.; Calderone, A.; Lazzaroni, R.; Brédas, J. L. *Chem.—Eur. J.* **2000**, *6*, 3739.
(74) Padowitz, D. F.; Messmore, B. W. *J. Phys. Chem. B* **2000**, *104*, 9943.
(75) Padowitz, D. F.; Sada, D. M.; Kemer, E. L.; Dougan, M. L.; Xue, W. A. *J. Phys. Chem. B* **2002**, *106*, 593.
(76) Leininger, S.; Olenyuk, B.; Stang, P. J. *Chem. Rev.* **2000**, *100*, 853.
(77) If the center of the molecule is used for the calculation of the angles, then the uracilic groups are positioned at 69° and 111° relative to each other.
(78) Wetterer, S. M.; Lavrich, D. J.; Cummings, T.; Bernasek, S. L.; Scoles, G. *J. Phys. Chem. B* **1998**, *102*, 9266.
(79) Zacharia, R.; Ulbricht, H.; Hertel, T. *Phys. Rev. B* **2004**, *69*, 155406.
(80) Palma, C. A.; Bonini, M.; Llanes-Pallas, A.; Breiner, T.; Prato, M.; Bonifazi, D.; Samorì, P. *Chem. Commun.* **2008**, 5289.
(81) Kampschulte, L.; Werblowsky, T. L.; Kishore, R. S. K.; Schmittel, M.; Heckl, W. M.; Lackinger, M. *J. Am. Chem. Soc.* **2008**, *130*, 8502.
(82) Palma, C. A.; Bonini, M.; Breiner, T.; Samorì, P. *Adv. Mater.*, in press.
(83) Sonogashira, K.; Tohda, Y.; Hagihara, N. *Tetrahedron Lett.* **1975**, *16*, 4467.

Scheme 1[a]

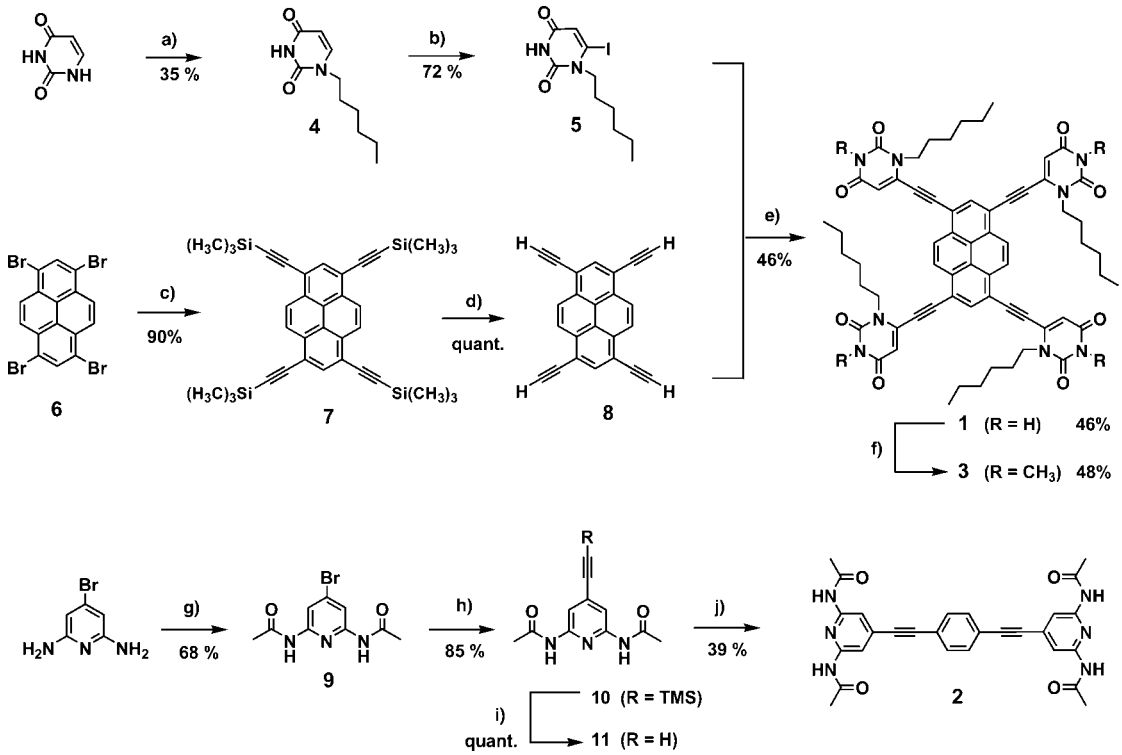

[a] (a) 1-Bromohexane, K_2CO_3, DMSO, 40 °C, 20 h; (b) LDA, THF, −78 °C, 1.5 h, then I_2, 2 h, then AcOH, rt, 10 h; (c) TMSA, $[Pd(PPh_3)_2]$, CuI, PPh_3, *i*-Pr_2NH, THF, 80 °C, 12 h; (d) 1 M (aq) KOH, 1:1 MeOH/CH_2Cl_2, rt, 40 min; (e) $[Pd(PPh_3)_4]$, CuI, Et_3N, THF, 45 °C; (f) DMSO, KOH, MeI; (g) Ac_2O, pyridine, rt, 10 h; (h) TMSA, $[Pd(PPh_3)_4]$, CuI, NEt_3, THF, reflux, 12 h; (i) 1 M (aq) KOH, MeOH, rt, 40 min; (j) 1,4-diiodobenzene, $[Pd(PPh_3)_4]$, CuI, NEt_3, THF, reflux, 12 h. Abbreviations: DMSO, dimethyl sulfoxide; LDA, lithium diisopropylamine; THF, tetrahydrofuran; TMSA, trimethylsilylacetylene.

sponding aromatic cores. Module **1**, bearing four uracil recognition sites, was prepared in the following way. 1-Hexyluracil (**4**) was obtained by reaction of unsubstituted uracil with 1-bromohexane in the presence of K_2CO_3 and DMSO. Subsequent deprotonation of **4** with LDA and addition of I_2 afforded the C6-iodinated derivative **5**. In parallel, tetraethynylpyrene **7** was prepared by Sonogashira cross-coupling between 1,3,6,8-tetrabromopyrene (**6**) and trimethylsilylacetylene (TMSA) followed by cleavage of the TMS protecting groups upon addition of a 1 M aqueous solution of KOH. Reaction of 1,3,6,8-tetraethynylpyrene (**8**) with **5** in the presence of CuI and $[Pd(PPh_3)_4]$ afforded the final tetratopic 1,3,6,8-tetrakis[(1-hexylurac-6-yl)ethynyl]pyrene **1** as a dark-red powder, which was purified by repeated precipitation cycles and characterized by ^1H and ^{13}C NMR spectroscopy in pyridine-d_5. Molecule **1** proved to be scarcely soluble in most organic solvents because of the extended homomolecular double H-bonding interactions established between the peripheral uracil moieties. In order to comprehensively characterize the compound, we methylated the imidic functionalities by reacting the tetrauracil module **1** with MeI in the presence of KOH. As expected, the introduction of the methyl groups at the imidic positions afforded the tetramethylated derivative **3**, which proved to be extremely soluble in $CHCl_3$, and thus easily characterized. Ditopic module **2** was synthesized following a similar approach to that utilized for **1**, using the Pd-catalyzed cross-coupling reaction between 4-ethynyl-2,6-diacetylaminopyridine (**11**) and 1,4-diiodobenzene. 4-Ethynyl-2,6-diamidopyridine was prepared in three steps starting from 4-bromo-2,6-diaminopyridine. Acetylation of 4-bromo-2,6-diaminopyridine with Ac_2O in pyridine yielded product **9**, which was subsequently cross-coupled with TMSA using $[Pd(PPh_3)_4]$/CuI in the presence of Et_3N to yield the TMS-protected acetylene derivative **10**. Subsequent treatment of **10** with aqueous KOH in MeOH afforded **11**, which was coupled to 1,4-diiodobenzene via Sonogashira reaction. All of the compound structures were assessed by electrospray ionization (ESI) mass spectrometry and ^1H and ^{13}C NMR, UV−vis, and IR spectroscopies. Module **1**, possessing pseudofourfold symmetry with two different angularities (120° and 60°), could lead to several polygonal arrangements when assembled with molecule **2** (Figure 1). In particular, the assembly of module **2** with (*a*) six angular modules **1** through twelve latitudinal uracil sites, (*b*) three angular modules **1** through six longitudinal uracil sites, and (*c*) four angular modules **1** through four longitudinal and latitudinal uracil sites, could in principle yield hexagonal, triangular, and rhomboidal structures, respectively.

Self-Recognition Behavior of 2D Oligomers in Solution: UV/Vis Absorption and Emission Measurements. The poor solubility of the H-bonding modules **1** and **2** (Figure 1) in aprotic solvents did not allow us to study the self-assembly process in solution by ^1H NMR spectroscopy. Nevertheless, the low concentration ($\sim 10^{-6}$ M) required by the spectroscopic analysis allowed a titration study of the self-assembly process in solution using UV/vis and fluorescence spectroscopies. Molecules **1** and **2** are strong absorbers in the UV region, with maxima at 345 nm ($\varepsilon = 37\,500\ M^{-1}\ cm^{-1}$) and 324 nm ($\varepsilon = 40\,600\ M^{-1}\ cm^{-1}$), respectively, in DMSO (Figure 2). 1,3,6,8-Tetrasubstituted pyrene **1** also exhibits an extended absorption envelope in the visible spectral region peaked at 481 nm ($\varepsilon = 37\,700\ M^{-1}\ cm^{-1}$)[84] that does not overlap with the spectral features of linear module **2**. This mismatching proved to be of crucial importance

(84) Maeda, H.; Maeda, T.; Mizuno, K.; Fujimoto, K.; Shimizu, H.; Inouye, M. *Chem.—Eur. J.* **2006**, *12*, 824.

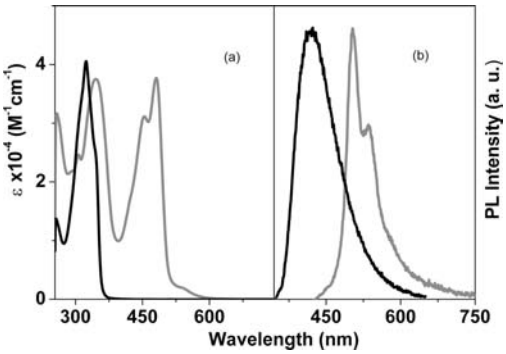

Figure 2. (a) Absorption spectra of **1** (gray line) and **2** (black line) in DMSO. (b) Normalized fluorescence spectra of **1** (gray line) and **2** (black line) in DMSO using $\lambda_{exc} = 308$ nm.

for performing optical titrations because it enabled excitation selectivity and easy attribution of spectral changes. Both **1** and **2** are relatively strong emitters, with fluorescence bands exhibiting maxima at 503 nm ($\Phi_{fluor} = 0.26$) and 423 nm ($\Phi_{fluor} = 0.10$), respectively, in DMSO (Figure 2). The related singlet lifetimes are 1.5 ns for **1** and 1.2 ns for **2**.

The H-bonding-based molecular recognition process between modules **1** and **2** can be monitored in solution by taking advantage of the strong chromophoric and emissive character of the two molecules, provided that a solvent that does not compete with formation of H-bond is utilized. This turned out to be particularly challenging because of the poor solubility of 1,3,6,8-tetrasubstituted pyrene **1** in many organic solvents. Indeed, attempts made in mixtures of CCl_4 or CH_2Cl_2 with DMSO, in which molecule **1** is soluble, gave no evidence of association. Finally, a clear proof of molecular recognition was obtained in a 1:50 DMSO/1,2,4-trichlorobenzene solution. Under these conditions, addition of increasing amounts of linear module **2** to a 8.4×10^{-6} M solution of pyrene **1** caused dramatic changes in the absorption and fluorescence spectra. Two different stages can be traced: 0−1 equiv (Figure 3a) and 1−2.4 equiv (Figure 3c) of compound **2**.

Upon addition of 1 equiv of molecule **2**, the visible absorption spectrum of pyrene **1** undergoes significant changes, and clean isosbestic points are found at 435 and 497 nm (Figure 3a). The former is slightly shifted to 427 nm upon further addition of molecule **2** (up to 2.4 equiv, Figure 3c). At 2.5 equiv or higher, extensive formation of suspended aggregates occurs. Parallel to the changes in the absorption spectra, substantial variations of the fluorescence profiles occur during the titration. During the initial stage (Figure 3b) the strong green fluorescence signal of the pyrene derivative is decreased by 80% and a novel emission band, peaked at ~570 nm, grows in with an isoemissive point at 593 nm. During the second titration step, the pyrene-centered fluorescence signal is further decreased to less than 4% of its initial value, whereas the intensity of the new emission band is affected only slightly or not at all (Figure 3d). Notably, the isoemissive point observed during the first stage of the titration is lost, pointing to the formation of more than one emissive species.

The interpretation of these data in solution is not straightforward since tetratopic (**1**) and ditopic (**2**) assembling modules are involved, with the H-bonding recognition sites rather distant from each other, thus favoring independent complexation of four

(85) Deleted in proof.

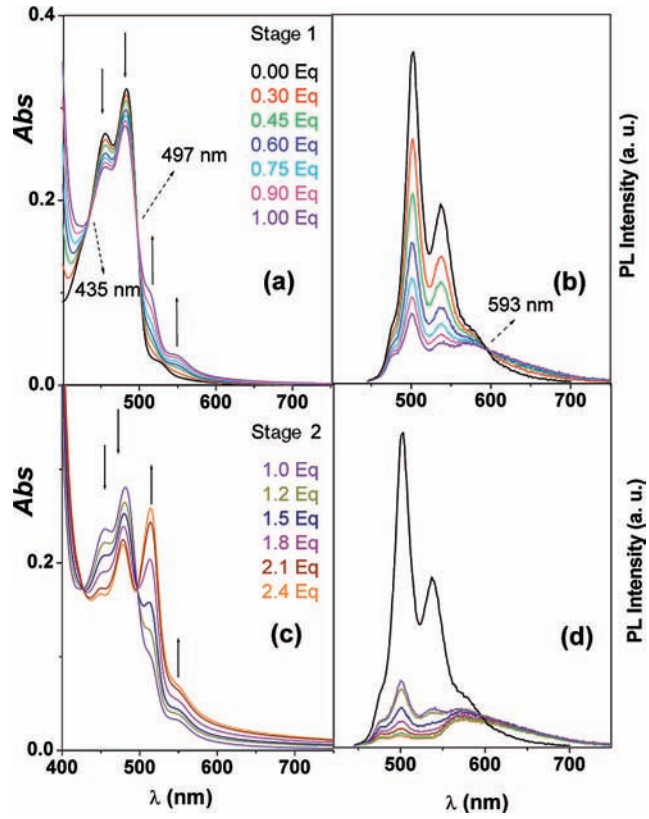

Figure 3. Changes of the absorption (left) and fluorescence (left) spectra of a 8.4×10^{-6} M solution of module **1** in 1:50 DMSO/1,2,4-trichlorobenzene upon addition of increasing amounts of linker **2** (from 0 to 2.0×10^{-5} M): (a, b) stage 1; (c, d) stage 2. Dashed arrows in (a) and (b) indicate isosbestic and isoemissive points, respectively. $\lambda_{exc} = 430$ nm, at which the absorbance value is virtually constant throughout the entire titration.

complementary DAD binding units. During the initial stage of the titration, the substantial decrease in the pyrene-centered fluorescence intensity (~80%, Figure 3b) suggests that a large majority of the pyrene derivatives are bound to at least one unit of the linear module[86] (Scheme 2). This likely occurs through a variety of associations between molecules **1** and **2** that give rise to clean isosbestic points because the binding sites are independent of each other.[87] The supramolecular adducts are soluble up to the addition of ~2 equiv of the linear ditopic module **2**. However, when larger amounts of **2** are added to a solution of pyrene **1**, the progressive formation of a solid suspension is observed. Starting from 2.5 equiv of molecule **2**, the aggregation process becomes so extensive that the optical transparency of the solution is no longer suitable for performing reliable spectroscopic measurements, and precipitation also occurs. This finding underpins the progressive formation of large supramolecular oligomers/networks that are insoluble in solution.

(86) The observed luminescence quenching of the pyrene derivative can occur only via intramolecular interactions, since intermolecular quenching processes must be ruled out because of the short singlet lifetime of **1** (1.5 ns) and the low concentration of the added component **2** ($< 1.0 \times 10^{-5}$ M). Moreover, energy-transfer quenching of **1** by **2** is thermodynamically not allowed, as can be derived by the relative spectral location of the fluorescence bands.

(87) It is worth emphasizing that optical studies in solution do not evidence self-aggregation of **2**. No absorption and emission spectral changes were detected in the DMSO/trichlorobenzene solvent mixture when the concentration of **2** was increased from 8.4×10^{-6} to 2.1×10^{-5} M (the same concentration range as in the titration experiment).

Scheme 2. Tentative Interpretation of the H-Bonding Recognition Process during the Titration Studies and Formation of Noncyclic Dimeric **1·2** and Trimeric **1·(2)$_2$** Assemblies

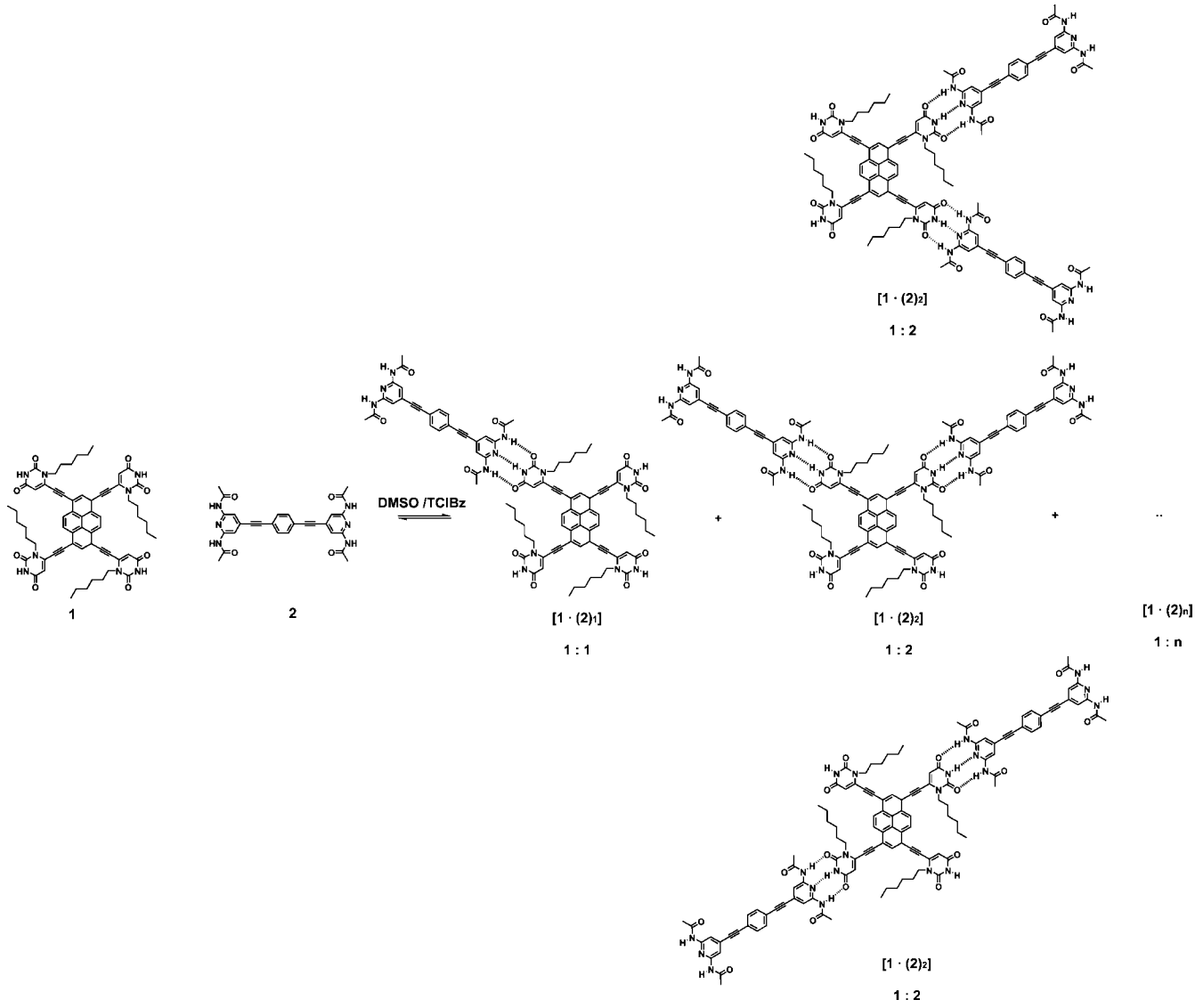

The red-shifted, weaker emission band that grows up during the titration could be assigned to H-bonded structures in solution. It could be argued, however, that its shape and position are reminiscent of excimer-type bands, which are normally observed for pyrene derivatives in solution at relatively high concentration ($>10^{-4}$ M).[88] This excimer assignment can be ruled out because the excitation spectrum recorded at the end of the titration at 585 nm (see Figure S1 in the Supporting Information) matches the features observed in the absorption spectrum (e.g., the 515 nm peak), supporting the hypothesis that the novel emitting species are also found in the electronic ground state and not only in the excited state, as would be observed for excimers.

As far as excited-state lifetimes are concerned, the singlet lifetime of the residual pyrene-centered signal during the first titration stage (0−1 equiv of **2**) is unchanged relative to the initial value (1.5 ns), whereas the new red-shifted signal exhibits a multiexponential emission decay. The related lifetime values are slightly dependent on the monitored emission wavelength but are never longer than 6.5 ns; thus, they are shorter than the lifetime of the intrinsic excimer emission of pyrene derivative **1** recorded at 10^{-3} M (29 ns). These results indicate that the H-bonded complexes, albeit exhibiting identical absorption spectra (see above), do show slightly different excited-state properties. This trend is confirmed at the end of stage 2 (at ∼2 equiv), where it is possible to selectively excite the supramolecular assemblies at their new absorption features, e.g., at 515 nm (Figure 4). The wide, irregular emission profile suggests the formation of multiple H-bonded oligomeric species with slightly modulated fluorescence spectra, reflecting the presence of various aggregates between the two polytopic receptors that exhibit different electronic delocalization as a function of the aggregate size. The presence of multiple species is confirmed by luminescence lifetime decays that are fitted as double/multiple exponentials with wavelength-dependent amplitudes (Figure 4).

The noticeable red shift of the pyrene-centered absorption and emission features suggests substantial electronic delocalization in the supramolecular structures formed upon titration. This might occur via either H-bonding interactions between molecules **1** and **2** or $\pi-\pi$ stacking between the 1,3,6,8-

(88) Birks, J. B. *Photophysics of Aromatic Molecules*; John Wiley and Sons: New York, 1970.

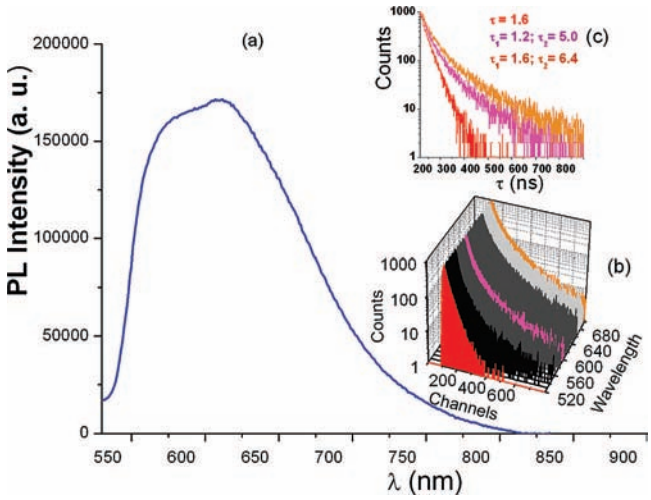

Figure 4. (a) Fluorescence spectrum (λ_{exc} = 515 nm) of a solution containing pyrene derivative **1** (8.4×10^{-6} M) and linker **2** (2.0×10^{-5} M) in 1:50 DMSO/1,2,4-trichlorobenzene at the end of the titration experiment (2.4 equiv of **2** added). (b) Luminescence decays as a function of the emission wavelength. (c) Emission decays recorded at three selected wavelengths: (red) 520, (magenta) 600, and (orange) 700 nm.

tetrasubstituted pyrene moieties belonging to different oligomeric assemblies. The sharp bands of the absorption spectrum at the end of the second stage tend to support the former hypothesis. On the other hand, $\pi-\pi$ stacking aggregates of aromatic molecules usually give weak and broad absorption tails on the red edge of the spectrum,[89] which, in our case, could be masked by the absorption background tail caused by the formation of a solid suspension (see above). It cannot be excluded that insoluble aggregates could be generated by the combined formation of larger and larger H-bonded oligomers that also undergo intermolecular stacking between the pyrene units.[90] At any molar ratio, the H-bonding interactions are essential for inducing the formation of supramolecular assemblies, as evidenced by a control experiment carried out with the methyl-capped 1,3,6,8-tetrasubstituted pyrene derivative **3**, which cannot undergo triple H-bonding interactions with linker **2**. Upon titration of **3** with linear module **2** under the same conditions as described in Figure 3 for molecules **1** and **2**, neither absorption/emission spectral changes nor formation of insoluble aggregates are observed, also ruling out the possibility of stacking interactions between the two different molecules (see Figure S2 in the Supporting Information). Very importantly, all of the spectral changes observed during the titrations are fully reversible. By addition of a few drops of DMSO, which disrupts the intermolecular H-bonds, a full recovery of the pyrene-centered absorption and fluorescence features is observed, and the precipitated assemblies are promptly and completely dissolved (see Figure S1 in the Supporting Information).

Self-Recognition Behavior of 2D Oligomers at the Solid−Liquid Interface. STM Investigations. While there are many reports on 2D supramolecular oligomers/polymers imaged via STM, whose structures rely on the ability of the molecules to form self-assembled crystalline patterns, rare are those reports in which the organization is solely dictated by the structural information embedded within the molecular modules, i.e., where the substrate plays a negligible role in dictating the final symmetry of the assembly. Unambiguous interpretation of the self-assembled patterns can be made provided that submolecular resolution is achieved. Furthermore, most studies involve self-assembled patterns that are dictated by the surface and do not exist (or have not been proved to exist) in solution. A strategy based on concentration control can be employed to accurately visualize the formation of bicomponent 2D supramolecular oligomers at an interface and compare them to the 2D supramolecular oligomeric motifs nucleated in solution. Given the difference in adsorption energies of the components and the tendency to minimize the occupied area, it is possible to set a threshold of concentration in which there cannot be competitive adsorption. Thus, we operate in a regime where the assembly is mostly dominated by the highly directional intermolecular interactions and where substrate−molecule interactions contribute less to the determination of phase formation.[80−82] This approximation holds as long as the molecule−solvent interactions are negligible. By setting the concentration around or below that necessary to form a densely packed monolayer of the different molecular patterns, we can ensure that the minimization of the global interfacial energy (yielding the thermodynamically stable phase) depends only on the intermolecular energies between assemblies **1·1**, **2·2**, and **1·2**. It is noteworthy that the interface concentration is a function of the interfacial area, which depends experimentally on the area wetted by the solution. This approach is somewhat analogous to that used for ultrahigh vacuum STM experiments, where polymorphism in multicomponent networks is avoided through a careful control of the stoichiometry of the components deposited on the surfaces.[24] In order to prove this concept, we have imaged the constitutive components of the supramolecular 2D oligomers at submonolayer concentrations. Notably, the concentrations are in the micromolar range, and the solvent used for imaging is 1,2,4-trichlorobenzene; these are the same conditions used for the formation of the bicomponent oligomers in solution. The DMSO content in the STM solutions, which was needed to solubilize the starting material, was kept near that used for the optical studies (1−0.1%). For the sake of comparison, the patterns at high concentration have also been imaged and reported. Figure 5a,b displays the surface-confined pattern of a monolayer of pyrene conjugate **1** prepared by depositing 5 μL of a diluted solution (concentration <10 μM). In the high-resolution image (Figure 5b), individual molecules within the ordered pattern can be identified by their characteristic cross shape: the central bright spot corresponds to the pyrene aromatic core and the lateral protrusions correspond to the uracil aliphatic chains. The contrast is ruled by resonant tunneling between the Fermi level of the HOPG substrate and the frontier orbitals of the adsorbed molecules.[91] From the proposed model, it clearly appears that neighboring molecules interact with each other through the formation of homomolecular coupling that occurs via the coexistence of two parallel H-bonds between their peripheral uracil moieties. The same packing was obtained from more concentrated solutions (>100 μM) (image not shown). In view of the area of the unit cell occupied by a single molecule of **1**, which amounts to 4.95 ± 0.06 nm^2, and the fact that the crystalline domains are extended over several hundreds of square nanometers, it is possible to estimate that 5 μL of a 10 μM solution contains ~1.5 times the number of molecules needed to form a densely packed monolayer on 1 cm^2 of HOPG. The

(89) Würthner, F.; Thalacker, C.; Sautter, A. *Adv. Mater.* **1999**, *11*, 754.
(90) Würthner, F.; Hanke, B.; Lysetska, M.; Lambright, G.; Harms, G. S. *Org. Lett.* **2005**, *7*, 967.
(91) Lazzaroni, R.; Calderone, A.; Brédas, J. L.; Rabe, J. P. *J. Chem. Phys.* **1997**, *107*, 99.

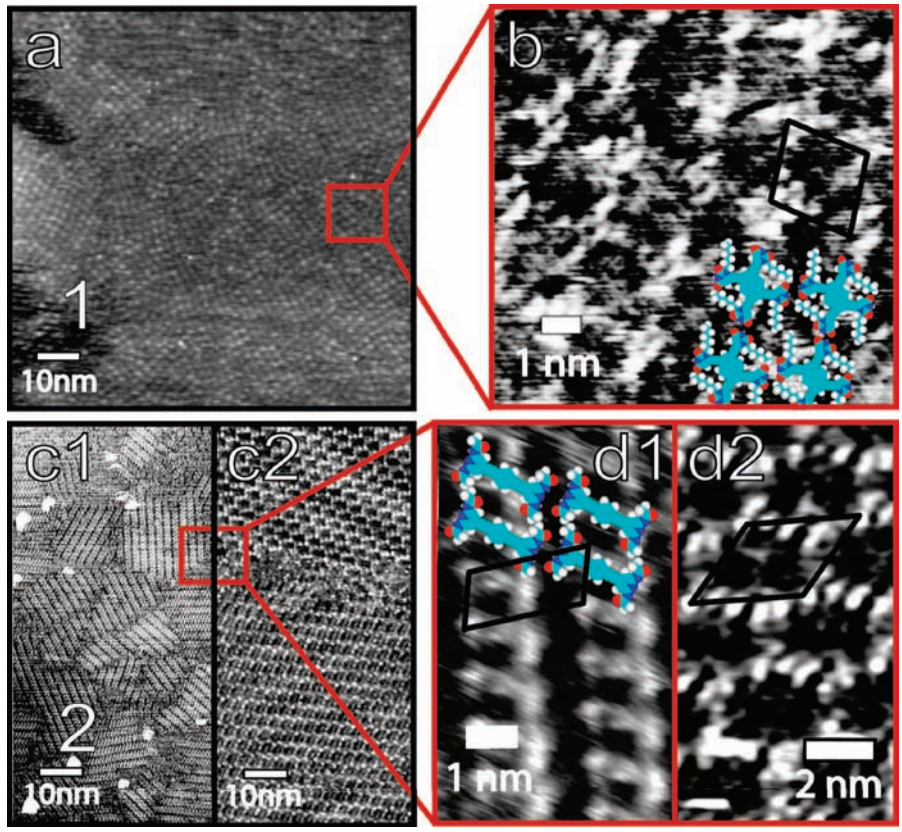

Figure 5. Constant-current STM images of monocomponent monolayers of physisorbed molecules: (a, b) **1**; (c, d) **2.** The high-resolution images show the unit cells: (b) $a = 2.3 \pm 0.1$ nm, $b = 2.2 \pm 0.1$ nm, $\alpha = 80 \pm 4°$; (d1) $a = 1.0 \pm 0.2$ nm, $b = 2.5 \pm 0.1$ nm, $\alpha = 65 \pm 4°$; (d2) $a = 3.3 \pm 0.2$ nm, $b = 3.9 \pm 0.1$ nm, $\alpha = 47 \pm 2°$. The average tunneling current was $I_t = 20$ pA, and the sample bias U_t was between 400 and 800 mV.

molecules in excess (i.e., those not adsorbed at the solid−liquid interface) are solvated in the 3D supernatant solution. On the other hand, molecule **2** was found to physisorb from diluted (<10 μM) solutions on HOPG into two different and coexisting self-assembled networks (Figure 5c1,c2). In the STM image (Figure 5d), individual molecules **2** can be identified in view of their characteristic linear shape, where three aligned bright lobes can be discerned (Figure 5d1). Each lobe can be attributed to an aromatic core: the central one corresponds to the 1,4-disubstituted phenyl moiety, whereas the peripheral functions correspond to the 2,6-di(acylamino)pyridyl substitutents. The first network (Figure 5c1,d1; unit cell: $a = 1.0 \pm 0.2$ nm, $b = 2.5 \pm 0.1$ nm, $\alpha = 65 \pm 4°$) shows a lamella-type motif. While molecule−molecule interactions at the intralamellar level are of the van der Waals type, at the interlamellar level they consist of H-bonding. In the second network (Figure 5c2,d2; unit cell: $a = 3.3 \pm 0.2$ nm, $b = 3.9 \pm 0.1$ nm, $\alpha = 47 \pm 2°$), the molecules arrange in a distorted hexagonal structure. The self-assembly is likely to be driven by the interplay of van der Waals and H-bonding interactions, but the exact packing could not be elucidated from the STM images. Statistical grain analysis of the STM constant-current images reveals that the apparent pores possess a projected surface area of 2.2 nm^2. Notably, the same two patterns were also observed by applying highly concentrated solutions (>100 μM) to the surface.

Significantly, the STM images of the self-assembled pattern obtained from films prepared by depositing equimolar mixtures of modules **1** and **2** on HOPG from concentrated solutions (concentration >100 μM) (see Figure S3a,b in the Supporting Information) exactly match that obtained for neat films composed of linear unit **2** (Figure 5c2), featuring a unit cell with $a = 3.1 \pm 0.2$ nm, $b = 3.7 \pm 0.2$ nm, and $\alpha = 50 \pm 3°$. This indicates that the formation of a molecule **2**-based monolayer is thermodynamically favored. It should be noted that no coexisting structured domains containing molecule **1** were found in over 100 survey images (i.e., mapping an area of 10^4 nm^2). Therefore, under these conditions, molecule **1** remains in the supernatant solution. To avoid such a fractionation, we opted to operate in a kinetically controlled regime, i.e., by using a concentration below that needed to form a full monolayer.[40] The use of very low concentration solutions (<10 μM) allowed the simultaneous physisorption of the solutes at the solid−liquid interface, preventing unfavorable thermodynamically driven competitive adsorption between modules **1** and **2**. As expected, for concentrations below 10 μM, a new **1·2** heterogeneous hybrid phase appears (Figure 6; large-area images are shown in Figure S3c,d in the Supporting Information). Such a heterogeneous phase was also found to coexist with the two packing modes of molecule **2**, which in this case are in the minority. We remark that the different phase coverages of the **1·2** phase varied in different experiments and that a trend could not be established. This was true even when employing ratios of 1:1, 1:2, 1:4, and 1:6 at different concentrations (from ~0.02 to ~6 μM) of molecules **1** and **2**, respectively. When some samples were annealed (~50 °C, ~2 min), phases of molecule **2** only were encountered. This further confirms that a monocomponent assembly is the thermodynamically stable phase and that the imaging of the heterogeneous phase is kinetically controlled. This kinetic control at low concentrations further extends the hypothesis that the 2D oligomeric species are created in solution and then directly transferred to the surface.

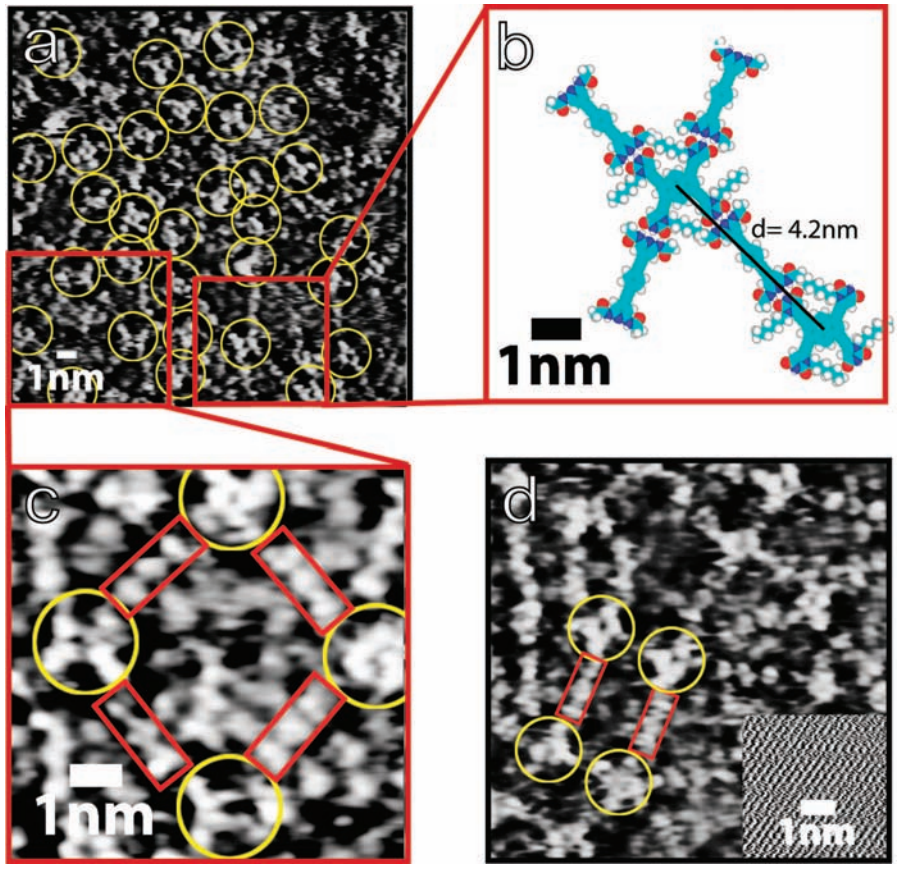

Figure 6. (a) Submolecularly resolved supramolecular aggregates featuring discrete oligomeric species $(\mathbf{1})_m\cdot(\mathbf{2})_n$ prepared from diluted equimolar solutions. Each yellow circle identifies a single molecule of tetrasubstituted 1,3,6,8-pyrene derivative **1**. (b) Model assembly of a hexameric hybrid complex $(\mathbf{1})_2\cdot(\mathbf{2})_4$ showing the distance values as estimated by MM2-based computational geometry optimization. (c, d) Heterogeneous **1·2** phase images highlighting the presence of rhomboidal and rectangular nanopolygons, respectively, formed as a consequence of complementary H-bonding motifs between molecules **1** and **2**. Each yellow circle identifies a single molecule of **1** and each red rectangle a single molecule of **2**. The inset in (d) shows the underlying graphite. All of the constant-current STM images where recorded with $I_t = 20$ pA and $U_t = 400$ mV.

Only when high-resolution images of the **1·2** heterogeneous phase (Figure 6) are obtained modules **1** and **2** can be unequivocally assigned after close inspection. The images reveal several polygon-like oligomeric species featuring hollow structures in line with the geometries shown in Figure 1. The high adsorption energies of the modules are also evidenced: polygons featuring large pore areas (Figure 6c) contain adsorbed molecules of **2**. Pores featuring small areas appear to be empty of solute molecules (Figure 6d). As described in the Introduction, the structures of the supramolecular complexes are dictated by the predesigned geometries of the constituent molecular modules. In particular, the structural fingerprints of the single modules can be easily discerned within the formed oligomers. Tetratopic pyrene **1** is imaged (yellow circles) as a bright spot exposing four arms, whereas ditopic linker **2** (red rectangles) features three aligned bright lobes. The formation of polygonal assemblies composed of complementary molecules **1** and **2** indicates that H-bonding interactions have been established. However, STM image analysis revealed a low percentage of molecules forming H-bonded pentamers (i.e., one molecule **1** surrounded by four H-bonded molecules of type **2**), as depicted in Figure 6b, namely, ~0.08 pentamers/nm^2 as estimated from 10 different images from different samples. The average angles γ and β in the pentamers relative to the pyrene center, as determined from the STM images, amount to 71 ± 8 and 110 ± 7°, respectively. Indeed, there is some slight discrepancy from the theoretical angles of 60° and 120° defined relative to the uracil groups because of the elongated pyrene unit. Furthermore, the average distance between two pyrene units in a linear **1·2·1** oligomer was found to be 4.3 ± 0.4 nm, which is in good agreement with the theoretical value of 4.2 nm estimated by MM2-based geometry optimization (Figure 6b). It is noteworthy that once they were formed, the supramolecular oligomeric motifs revealed to be stable for several minutes; thus, no self-healing phenomena were observed on the time scale of the experiment (see Figures S4 and S5 in the Supporting Information). Notably, some homomolecular **1·1** and **2·2** complexes were also observed as coexisting phases. Our STM studies have provided fundamental information on the design and engineering of supramolecular discrete patterns at interfaces. Even when competitive adsorption is prevented by using low concentrations, the supramolecular (**1·2**) oligomers cannot ripen into a thermodynamically stable self-assembled 2D crystalline pattern for two reasons: (*i*) module **1** is not centrosymmetric, so competing phenomena involving the different nucleating nanopolygons in Figure 6 exist; (*ii*) the monocomponent phase formed by **2** intrinsically appears to be the thermodynamically favored assembly. We have revealed that it is possible to resolve submolecularly amorphous 2D phases, which can serve as a powerful tool for the study of crystallization phenomena. In such phases, STM can locally probe the dynamics of single molecules (see Figures S4 and

S5 in the Supporting Information), which are relatively decoupled from a densely packed monolayer.

Conclusions

In summary, we have engineered nanoscale assemblies in solution and on surfaces through the design of programmed molecular modules that undergo heteromolecular recognition through complementary triple H-bonds. In particular, two molecular modules have been synthesized: a linear unit **2** having twofold symmetry with two exposed 2,6-di(acylamino)pyridyl (DAD) recognition sites at its extremities and an angular unit **1** constituted by a 1,3,6,8-tetraethynylpyrene core peripherally functionalized with four uracil groups (ADA) positioned at 60° and 120° relative to each other. Steady-state UV/vis absorption and emission titration measurements showed the reversible formation of multiple H-bonded oligomeric species in solution. At the end of the titration of **1** with **2**, novel absorption and fluorescence features were detected; by means of several control experiments including excitation spectra, these were unambiguously attributed to supramolecular aggregates, likely exhibiting a variety of association ratios between the two components. Careful analysis of electronic spectroscopy data allows us to conclude that in the ground state, H-bond formation between the ditopic molecule **2** and the tetratopic module **1** is substantially independent for the various sites, which are rather far apart. On the other hand, fluorescence spectra and singlet lifetimes indicate the presence of multiple species, suggesting distinctive properties in the excited state. After the addition of more than 2.4 equiv of linear module **2** to solutions of pyrene **1**, suspended aggregates and precipitates attributed to the generation of increasingly larger supramolecular arrays were observed. Despite the fact that other intermolecular interactions can occur (e.g., $\pi-\pi$ stacking), it has been demonstrated that complementary H-bonding is essential for the formation of supramolecular adducts in solution, because unique spectral variations are observed when both DAD and ADA fragments are present. Control of the experimental conditions allowed us to transfer such supramolecular oligomers from solution into the solid−liquid interface. This made possible the imaging of the 2D oligomers in real space, allowing the identification of higher-order structures and showing the expected formation of nanoscale polygons. Images of the **1·2** heterogeneous phase revealed that the overall formation of all of the supramolecular systems is primarily driven by the noncovalent yet highly directional and selective triple H-bonding interactions established between the complementary DAD and ADA recognition sites and by the geometrical molecular constraints, leading to several polygon-like arrays matching the preprogrammed geometries. We have highlighted the distinctive roles of self-healing, interfacial free energy, nucleation, and competing phenomena within 2D assemblies, which in turn dictate the ripening of the oligomeric species into ordered or disordered phases. Our observations allowed us to suggest that oligomers are nucleated in solution and transferred to interfaces without altering the nature of their directing interactions. A formal study of the mechanisms underlying the adsorption of single molecules or complete oligomeric species requires the development of in-situ spectroscopic techniques at the solid−liquid interface. Our findings and suggestions are of paramount importance for the continuous development of the field of 2D crystal engineering. Although further improvements are needed in order to strengthen the stability and the homogeneity of the assemblies, these nanopolygons could be employed as two-dimensional receptors to selectively incorporate suitable designed functional molecules that can interact with an external signal, exploiting desired functional activities.

Experimental Section

Synthesis. NMR spectra were obtained on a Varian Gemini 200 spectrometer (200 MHz ^{1}H NMR and 50 MHz ^{13}C NMR) and on a JEOL JNM-EX400 spectrometer (400 MHz ^{1}H NMR). Chemical shifts (δ) are reported in parts per million using the solvent residual signal as an internal reference ($CDCl_3$, $\delta_H = 7.26$ ppm, $\delta_C = 77.16$ ppm; CD_3OD, $\delta_H = 3.31$ ppm, $\delta_C = 49.00$ ppm; C_5D_5N, $\delta_H = 7.19, 7.55, 8.71$ ppm, $\delta_C = 123.5, 135.5, 149.5$ ppm; $(CD_3)_2SO$, $\delta_H = 2.50$ ppm, $\delta_C = 39.52$ ppm). Coupling constants (J) are given in hertz. Each resonance multiplicity is described as *s* (singlet), *d* (doublet), *t* (triplet), *q* (quartet), *dd* (doublet of doublets), *m* (multiplet), or *br* (broad signal). IR spectra (KBr) were recorded on a Perkin-Elmer 2000 spectometer by Mr. Paolo de Baseggio. In regard to mass spectrometry (MS) measurements, ESI was performed on a PerkinElmer API1 instrument at 5600 eV and electron impact (EI) on a GCQ Finnigan Thermoquest ion trap at 70 eV, both at Università degli Studi di Trieste by Dr. Fabio Hollan. Melting points were measured on a Büchi SMP-20 apparatus. Chemicals were purchased from Aldrich, Fluka, and Riedel and used as received. Solvents were purchased from J.T.Baker and Aldrich and deuterated solvents from Cambridge Isotope Laboratories. The solutions were degassed usin "freeze−pump−thaw" cycles. The solvents CH_2Cl_2, toluene, THF, and NEt_3 were distilled from CaH_2, Na, Na/benzophenone, and CaH_2 respectively. Syntheses of 4-bromo-2,6-diaminopyridine,[92] 1,3,6,8-tetrabromopyrene,[93] and 1,3,6,8-tetraethynylpyrene[94] were performed according to literature procedures.

1-Hexyluracil (4). To a suspension of uracil (2.8 g, 25 mmol) in DMSO (30 mL), dry K_2CO_3 (3.8 g, 27.5 mmol) was added, and the suspension was stirred for 15−20 min. 1-Bromohexane (3.5 mL, 25 mmol) was added and the reaction mixture stirred for 20 h at 40 °C. The suspension was diluted with $CHCl_3$, washed with 0.1 M HCl solution (20 mL × 3), H_2O (20 mL × 2), and brine (20 mL), and dried over Na_2SO_4. The organic layer was concentrated and poured into cold hexane with vigorous stirring. The resulting precipitate was filtered and washed with cold hexane to afford compound **4** (1.79 g, 35%) as a white solid. Mp: 91−95 °C. ^{1}H NMR (200 MHz, $CDCl_3$): δ 10.1 (*br*, 1H, CON*H*CO); 7.1 (*d*, ^3J(H,H) = 7.9 Hz, 1H, COC*H*); 5.7 (*d*, ^3J(H,H) = 7.9 Hz, 1H, NC*H*); 3.7 (*t*, ^3J(H,H) = 7.4 Hz, 2H, $NCH_2(CH_2)_4CH_3$); 1.7 (*m*, ^3J(H,H) = 7.4 Hz, 2H, $NCH_2CH_2(CH_2)_3CH_3$); 1.3 (*m*, 6H, $N(CH_2)_2(CH_2)_3CH_3$); 0.9 (*t*, 3H, $N(CH_2)_5CH_3$). ^{13}C NMR (50 MHz, $CDCl_3$): δ 164.14; 150.93; 144.37; 101.92; 48.78; 31.24; 28.92; 25.98; 22.39; 13.91. IR ν (cm^{-1}): 3417.2; 3155.1; 3098.2; 3044.9; 2951.0; 2931.8; 2862.1; 2821.1; 1975.3; 1694.0; 1646.9; 1467.1; 1420.6; 1368.8; 1250.3, 1179.3; 989.5; 887.7; 816.5; 761.0; 726.0; 558.5. MS (70 eV, EI): found, 196 (M^+); calcd for $C_{10}H_{16}N_2O_2$, 196.09.

1-Hexyl-6-iodouracil (5). To a THF solution (55 mL) of 1-hexyluracil **4** (1.7 g, 8.7 mmol), LDA (24 mL of a 1.8 M solution, 43.5 mmol) was added dropwise, and the resulting solution was stirred under Ar at −78 °C for 1.5 h. I_2 (11 g, 43.5 mmol) was added and the reaction mixture stirred for 2 h. The solution was then treated with acetic acid (1.2 mL) and allowed to warm to room temperature (r.t.). The organic phase was diluted with $CHCl_3$ (30 mL), washed with saturated aqueous (sat. aq.) $NaHCO_3$ solution (30 mL × 3), sat. aq. Na_2SO_3 solution (30 mL × 3), and brine (30 mL), and dried over Na_2SO_4. Evaporation of the solvents in vacuo and purification of the crude product by column chromatography (CC) (5:5 AcOEt/cyclohexane) yielded compound **5** (2.02 g, 72%)

(92) Nettekoven, M. *Synlett* **2001**, 1917.
(93) Vollmann, H.; Becker, H.; Correll, M.; Streeck, H. *Justus Liebigs Ann. Chem.* **1937**, *531*, 1.
(94) Venkataramana, G.; Sankararaman, S. *Eur. J. Org. Chem.* **2005**, 4162.

as a white solid. Mp: 123−125 °C. ^{1}H NMR (200 MHz, $CDCl_3$): δ 8.6 (*br*, 1H, CON*H*CO); 6.4 (*s*, 1H, COC*H*); 4.0 (*t*, ^3J(H,H) = 8.1 Hz, 2H, NCH_2(CH$_2$)$_4$CH$_3$); 1.7 (*m*, ^3J(H,H) = 8.1 Hz, 2H, NCH$_2$CH_2(CH$_2$)$_3$CH$_3$); 1.3 (*m*, 6H, N(CH$_2$)$_2$(CH_2)$_3$CH$_3$); 0.9 (*t*, 3H, N(CH$_2$)$_5$CH_3). ^{13}C NMR (50 MHz, $CDCl_3$): δ 161.04; 148.02; 115.73; 113.92; 53.84; 31.46; 28.85; 26.14; 22.69; 14.17. IR ν (cm^{-1}): 3173.7; 3043.6; 1953.7; 2932.6; 2917.1; 2855.1; 1684.9; 1567.8; 1431.0; 1394.5; 1353.7; 1220.4; 1169.4; 1071.9; 1002.7; 827.4; 792.1; 750.9; 720.9; 635.4; 572.8; 537.0. MS (70 eV, EI): found, 322 (M^+); calcd for $C_{10}H_{15}IN_2O_2$, 322.14.

1,3,6,8-Tetrakis[(1-hexylurac-6-yl)ethynyl]pyrene (1). To a degassed solution of dry THF (5 mL) and NEt_3 (5 mL), 1-hexyl-6-iodouracil **5** (0.270 g, 0.84 mmol), [Pd(PPh$_3$)$_4$] (4 mg, 0.034 mmol), and CuI (13 mg, 0.068 mmol) were added, and the resulting mixture was degassed a second time. 1,3,6,8-Tetraethynylpyrene **8** (0.05 g, 0.17 mmol) was added, and the solution was degassed one last time and stirred overnight at 45 °C under Ar. After some minutes, the reaction color changed and a red precipitate appeared. The suspension was then concentrated in vacuo, and the crude product purified by several precipitations from $CHCl_3$ upon addtion of MeOH, yielding compound **1** (0.082 g, 46%) as a dark-red solid. ^{1}H NMR (400 MHz, C_5D_5N): δ 9.03 (*s*, 4 H, pyrene-*H*); 8.90 (*s*, 2H, pyrene-*H*); 6.64 (*s*, 4 H, COC*H*); 4.37 (*br*, 8 H, NCH_2(CH$_2$)$_4$CH$_3$); 2.01 (*m*, 8H, NCH$_2$CH_2(CH$_2$)$_3$CH$_3$); 1.53 (*m*, 8H, N(CH$_2$)$_2$CH_2(CH$_2$)$_2$CH$_3$); 1.31 (*m*, 16H, N(CH$_2$)$_3$(CH_2)$_2$CH$_3$); 0.81 (*t*, 12H, N(CH$_2$)$_5$CH_3). ^{13}C NMR (50 MHz, C_5D_5N): δ 169.67; 152.14; 137.85; 133.64; 131.88; 126.68; 121.41; 118.21; 109.09; 96.41; 88.86; 47.09; 32.13; 27.16; 26.32; 23.26; 14.53. IR ν (cm^{-1}): 3442.6; 3164.0; 3034.1; 2954.8; 2919.3; 2850.8; 2202.9; 1690.2; 1600.0; 1581.9; 1456.2; 1243.3; 1170.5; 1114.1; 825.2; 618.7. MS (5600 eV, ESI): found, 1075.4(M^+), 1098.3 $(M + Na)^+$; calcd for $C_{64}H_{66}N_8O_8$, 1075.26.

1,3,6,8-Tetrakis[(1-hexyl-3-methylurac-6-yl)ethynyl]pyrene (3). To a suspension of 1,3,6,8-tetrakis[(1-hexylurac-6-yl)ethynyl]pyrene **1** (0.03 g, 0.028 mmol) in DMSO, KOH powder (0.1 g, 1.78 mmol) was added, and the resulting mixture was stirred at r.t. for 15 min. MeI (0.04 mL, 0.64 μmol) was then added and the whole mixture allowed to stir at r.t. for 5 h. The resulting red solution was then diluted with $CHCl_3$ (5 mL), copiously washed with H_2O (5 mL × 5) and brine (5 mL × 2), and dried over Na_2SO_4. Removal of the solvent under vacuum and purification of the crude product by CC (9.8:0.2 CH_2Cl_2/MeOH) yielded compound **3** (0.015 g, 48%) as a red-orange oil. ^{1}H NMR (200 MHz, $CDCl_3$): δ 8.67 (*s*, 4H, pyrene-*H*); 8.45 (*s*, 2H, pyrene-*H*); 6.28 (*s*, 4H, COC*H*); 4.23 (*t*, 8H, NCH_2(CH$_2$)$_4$CH$_3$); 3.41 (s, 12H, N−CH_3); 1.89 (*m*, 8H, NCH$_2$CH_2(CH$_2$)$_3$CH$_3$); 1.6 (*m*, 8H, N(CH$_2$)$_2$CH_2(CH$_2$)$_2$CH$_3$); 1.33 (*m*, 16H, N(CH$_2$)$_3$(CH_2)$_2$CH$_3$); 0.82 (*t*, 12H, N(CH$_2$)$_5$CH_3). ^{13}C NMR (50 MHz, $CDCl_3$): δ 161.90; 151.37; 135.59; 134.95; 133.11; 127.86; 123.75; 117.51; 107.46; 95.97; 87.71; 48.00; 31.62; 29.16; 28.21; 26.64; 22.72; 14.15. IR ν (cm^{-1}): 3404.1; 2858.8; 2363.8; 2207.5; 1707.0; 1664.3; 1452.7; 1369.9; 1265.8; 1104.7; 810.7. MS (5600 eV, ESI): found, 1131.5 (M^+), 1153.5 $(M + Na)^+$; calcd for $C_{68}H_{76}N_8O_8$, 1131.36.

4-Bromo-2,6-diacetylaminopyridine (9). 4-Bromo-2,6-diaminopyridine (0.45 g, 2.14 mmol) was dissolved in a solution of pyridine (1.4 mL, 17.5 mmol) and Ac_2O (2.5 mL, 26.4 mmol), and the reaction mixture was stirred overnight at r.t. The mixture was then diluted with $CHCl_3$ (10 mL), washed with H_2O (10 mL × 5) and brine (20 mL), and dried over Na_2SO_4. Solvent evaporation and precipitation with Et_2O yielded compound **9** (0.44 g, 68%) as a yellow solid. Mp: 210−215 °C. ^{1}H NMR (200 MHz, 1:1 CD_3OD/$CDCl_3$): δ 7.7 (*s*, 2H, Ar−*H*); 4.3 (*s*, 2H, CH$_3$CON*H*−Ar); 1.9 (*s*, 6H, CH_3CONH−Ar). ^{13}C NMR (50 MHz, 1:1 CD_3OD/$CDCl_3$): δ 171.08; 151.20; 135.53; 112.67; 23.93. IR ν (cm^{-1}): 3311.5; 3124.7; 1685.7; 1577.9; 1538.1; 1415.5; 1367.2; 1280.8; 1237.7; 1199.7; 1035.0; 996.7; 861.4; 777.4; 746.9; 693.0; 603.0; 561.3; 549.1. MS (70 eV, EI): found, 273 (M^+); calcd for $C_9H_{10}BrN_3O_2$, 272.

2,6-Diacetylamino-4-[(trimethylsilyl)ethynyl]pyridine (10). Dry NEt_3 (40 mL), THF (6 mL), and DMF (1 mL) were added to a Schlenk tube, and the solution was degassed by one freeze−pump−thaw cycle. Diacetylamino pyridine derivative **9** (0.44 g, 1.6 mmol), [(Pd(PPh$_3$)$_4$] (0.074 g, 0.06 mmol), and CuI (0.024 g, 0.128 mmol) were added and the solution degassed a second time. TMSA (0.44 mL, 3.2 mmol) was then added, and the reaction mixture was degassed one last time and stirred overnight at 85 °C under Ar. The resulting dark mixture was filtered over Celite and washed with toluene (10 mL), CH_2Cl_2 (20 mL), and MeOH (20 mL). Removal of the solvents under vacuum and purification of the crude product by CC (5:5 cyclohexane/AcOEt) yielded compound **10** (0.4 g, 85%) as a yellow crystalline solid. Mp: 85−90 °C. ^{1}H NMR (200 MHz, $CDCl_3$): δ 8.4 (*br*, 2H, CH$_3$CON*H*−Ar); 7.8 (*br*, 2H, Ar−*H*); 2.0 (*s*, 6H, CH_3CONH−Ar); 0.2 (*s*, 9H, Si(CH_3)$_3$). ^{13}C NMR (50 MHz, $CDCl_3$): δ 168.36; 149.49; 135.88; 111.91; 102.44; 99.97; 24.83; 0.11. IR ν (cm^{-1}): 3422.9; 3276.1; 2960.2; 2161.9; 1681.5; 1611.9; 1557.9; 1416.0; 1370.0; 1276.1; 1249.7; 1206.9; 1145.0; 1033.4; 996.7; 983.5; 953.7; 848.1; 760.2; 705.1; 640.7; 625.8; 569.6; 539.3. MS (70 eV, EI): found, 289 (M^+); calcd for $C_{14}H_{19}N_3O_2Si$, 289.41.

2,6-Diacetylamino-4-ethynylpyridine (11). To a solution of TMS-protected ethynylpyridine derivative **10** (0.4 g, 1.38 mmol) in MeOH (15 mL), a 1 M KOH aq. solution was added, and the mixture was stirred at r.t. for 40 min. H_2O (10 mL) was added, and the organic phase was extracted with $CHCl_3$ (10 mL × 5) and dried over Na_2SO_4. Evaporation of the solvent under vacuum yielded compound **11** as a yellow crystalline solid in a quantitative yield. Mp: 208−213 °C. ^{1}H NMR (200 MHz, 1:1 CD_3OD/$CDCl_3$): δ 7.8 (*br*, 2H, Ar−*H*); 3.7 (*br*, 2H, CH$_3$CON*H*−Ar); 3.1 (*s*, 1H, C*H*); 2.0 (*s*, 6H, CH_3CONH−Ar). ^{13}C NMR (50 MHz, 1:1 CD_3OD/$CDCl_3$): δ 169.79; 149.79; 134.16; 111.72; 81.31; 24.09. IR ν (cm^{-1}): 3319.0; 3253.2; 3124.4; 2115.1; 1715.6; 1669.5; 1612.1; 1561.0; 1518.5; 1415.9; 1365.6; 1278.1; 1235.7; 1202.7; 1037.5; 998.8; 949.9; 876.0; 853.6; 724.9; 703.3; 673.7; 636.7; 562.4. MS (70 eV, EI): found, 217 (M^+); calcd for $C_{11}H_{11}N_3O_2$, 217.22.

4,4′-[(Phen-1,4-diyl)diethynyl]bis(2,6-diacetylaminopyridine) (2). To a degassed solution of dry Et_3N (10 mL) and THF (10 mL), 1,4-diodobenzene (0.07 g, 0.22 mmol), [Pd(PPh$_3$)$_4$] (0.01 g, 0.009 mmol), and CuI (3 mg, 0.018 mmol) were added and the mixture degassed a second time. Ethynylpyridine derivative **11** (0.120 g, 0.55 mmol) was then added, and the reaction mixture was degassed one last time and stirred overnight at 85 °C under Ar. After 1 h, a precipitate appeared. The solvent was then concentrated under vacuum and the precipitate purified by several precipitations from $CHCl_3$ upon addition MeOH, yielding compound **2** (0.9 g, 83%) as a pale yellow solid. Mp: >260 °C. ^{1}H NMR (400 MHz, DMSO-d_6): δ 10.25 (*s*, 4H, CH$_3$CON*H*−Ar); 7.9 (*s*, 4H, Ar−*H*); 7.7 (*s*, 4H, benzene-*H*); 2.1 (s, 12H, CH_3CONH−Ar). ^{13}C NMR (50 MHz, DMSO-d_6): δ 169.53; 150.69; 132.82; 132.13; 122.10; 110.26; 91.63; 89.54; 24.09. IR ν (cm^{-1}): 3296.7; 2217.3; 1672.3; 1612.1; 1557.6; 1416.4; 1370.3; 1278.8; 1239.6; 1205.7; 1026.9; 1002.3; 859.8; 629.3; 568.3. MS (5600 eV, ESI): found, 531.2 $(M + Na)^+$; calcd for $C_{28}H_{24}N_6O_4$, 508.53.

Photophysical Measurements. Solutions containing molecule **1** were prepared by dissolving a weighed amount of sample (1 mg) in a few drops of DMSO, in which it is soluble. Next, a much larger volume of 1,2,4-trichlorobenzene was added, in order to achieve a 1:50 volume ratio of the two solvents. Electronic absorption and emission measurements, respectively, were carried out on a Lambda 950 UV/vis/NIR spectrophotometer (PerkinElmer) and an Edinburgh FLS920 spectrofluorometer equipped with a continuous 450 W Xe lamp and a Peltier-cooled Hamamatsu R928 photomultiplier tube (185−850 nm). Emission quantum yields were determined according to the approach described by Demas and Crosby[95] using quinine sulfate as the standard (Φ_{em} = 0.546 in

(95) Demas, J. N.; Crosby, G. A. *J. Phys. Chem.* **1971**, *75*, 991.

air-equilibrated 1 N H_2SO_4 solution).[96] Emission lifetimes were determined with the time-correlated single-photon counting technique using an Edinburgh FLS920 spectrometer equipped with a laser diode head as the excitation source (1 MHz repetition rate, $\lambda_{exc} = 337$ nm, 200 ps time resolution upon deconvolution) and a Hamamatsu R928 PMT as the detector (details of the setup are reported elsewhere).[97] The fitting of the experimental data to single- or multiple-exponential decays was carried out with the software provided by the instrument manufacturer. Phosphorescence spectra and related long-lived decay signals were recorded with a PerkinElmer LS-50B spectrofluorimeter equipped with a Hamamatsu R928 PMT. The solvents used were 1,2,4-trichlorobenzene (Sigma-Aldrich, 99+% spectrophotometric grade) and dimethyl sulfoxide (Carlo Erba for UV-Fluo spectroscopy, 99.8%).

STM Studies at the Solid−Liquid Interface. Solutions were prepared by dissolving ~0.2 mg of **1** (1075 g/mol) or **2** (508 g/mol) in 50 μL of DMSO and 450 μL of trichlorobenzene (99% spectrometric grade, Alpha-Aesar). The solutions were heated at 90 °C to achieve complete dilution. The solutions were then diluted 5× in trichlorobenzene to obtain the high-concentration solutions (>100 μM) and 100× to obtain the low-concentration solutions (<10 μM). To prepare the high-concentration (>100 μM) **1·2** solutions, 100 μL of the starting solution of **1** was mixed with 50 μL of the **2** solution, and the volume was taken to 500 μL. To prepare the low-concentration (<10 μM) **1·2** solutions, 100 and 10 μL of the corresponding <10 μM solutions of **1** and **2**, respectively, were mixed. Next, 5 μL of the solutions were drop-cast onto HOPG. STM imaging at the solid−liquid interface was performed using a commercial apparatus (multimode Nanoscope III, Veeco) equipped with a low-current amplifier. First, the lattice of a freshly cleaved HOPG (001) surface (ZYH grade, Advanced Ceramics) was examined until thermal equilibrium was reached, after which a drop of the solution of interest was applied to the basal plane of the substrate. The Pt/Ir tip was then immersed in the organic solution. It was possible to visualize either the first organic layer physisorbed on the basal plane of the substrate or the HOPG lattice underneath by varying the tunneling parameters. All of the phases were imaged within the first 10 min of scanning and remained stable until complete solvent evaporation (~3 h). Submolecularly resolved images were recorded with a scan rate between 0.6 and 0.8 μm/s. The STM images were recorded in constant-current mode under ambient conditions. Unit cells were averaged over a minimum of three images after correction for the piezo drift, which was performed using the underlying graphite as reference and applying the correction to the image by means of the Scanning Probe Image Processor (SPIP) version 2.0 software (Image Metrology ApS, Lyngby, Denmark). Other image treatment included plane correction, contrast change, and low-weight low-pass filtering. Untreated images are shown in the Supporting Information. The reported error bars in the unit cells correspond to the standard deviation multiplied by a factor of 2. The size of the pores estimated by grain analysis did not take into account tip convolution effects. MM2-based optimization was performed with Chem3D Ultra 5.0.

Acknowledgment. This work was financially supported by the European Union through the Marie-Curie Research Training Network PRAIRIES (MRTN-CT-2006-035810) and EST-SUPER (MEST-CT-2004-008128), the CNR (Commessa PM.P04.010, MACOL), MIUR (Firb RBIN04HC3S), the Belgian National Research Foundation (FRS-FNRS, through Contract 2.4.625.08 F), the University of Namur, the ERA-Chemistry Project SurConFold, the ESF-SONS2-SUPRAMATES project, and the Regione Emilia-Romagna PRIITT Nanofaber Net-Laboratory. A.L.-P. thanks Università di Trieste for the doctoral fellowship.

Supporting Information Available: Figures S1−S5 and NMR and mass spectra of the synthesized compounds. This material is available free of charge via the Internet at http://pubs.acs.org.

JA807530M

(96) Meech, S. R.; Phillips, D. *J. Photochem.* **1983**, *23*, 193.
(97) Armaroli, N.; Accorsi, G.; Song, F.; Palkar, A.; Echegoyen, L.; Bonifazi, D.; Diederich, F. *ChemPhysChem* **2005**, *6*, 732.